Desalination and Water Treatment
www.deswater.com

doi: 10.5004/dwt.2018.21771

103 (2018) 72–83
January

Color removal for simulated nanofiltration concentrates of dye wastewater with iron ion supported nano-size silica microgel Fenton/coagulation processes

Chun Ming Zheng[a,*], ShuBin Chang[a], Dong Ying Lian[a], Hai Tao Wang[a], Chuan Wu Yang[a], Shi Jun Wei[a], Meng Wei Du[a], Shi Chao Xu[a], Xiao Hong Sun[b,*]

[a]*State Key Laboratory of Separation Membranes and Membrane Processes, School of Environmental and Chemical Engineering, Tianjin Polytechnic University, Tianjin 300387, China, Tel./Fax +86 022 83955661, email: zhengchunming@tjpu.edu.cn (C.M. Zheng), 1472451963@qq.com (S.B. Chang), 1761713372@qq.com (D.Y. Lian), wanghaitao@tjpu.edu.cn (H.T. Wang), 1558862045@qq.com (C.W. Yang), 773729641@qq.com (S.J. Wei), 1617213280@qq.com (M.W. Du), xushichao@tjpu.edu.cn (S.C. Xu)*
[b]*Key Laboratory of Advanced Ceramics and Machining Technology, Ministry of Education, School of Materials Science and Engineering, Tianjin University, Tianjin 300072, China, Tel./Fax +86 022 83955661, email: sunxh@tju.edu.cn (X.H. Sun)*

Received 7 April 2017; Accepted 6 December 2017

ABSTRACT

This article focuses on investigating the treatment efficiencies of nanofiltration concentrates by the silica coagulant combined with L-cysteine modified heterogeneous Fenton-like Fe(III) degradation (Cys-Fe(III)@mSiO$_2$). The structure and morphology of Cys-Fe(III)@mSiO$_2$ were characterized by scanning electron microscopy (SEM), transmission electron microscopy (TEM), X-ray diffraction (XRD), infrared spectra (FT-IR) and other characterizations. Fe(III) ions are uniformly dispersed on the Cys-Fe(III)@mSiO$_2$ microgel surface. The modification of L-cysteine to Fe(III)@mSiO$_2$ not only improved the silica-based coagulating efficiency but also expanded the degradation pH of heterogeneous Fenton-like Fe(III) reaction for nanofiltration concentrates. The degradation efficiencies of nanofiltration concentrates are also compared with Fe(II) and Fe(III) supported silica coagulants. The effective pH range of Cys-Fe(III)@mSiO$_2$ was expanded up to 6.5 and the color and COD degradation efficiencies reached above 90% and 85 % for simulated nanofiltration concentrates, which were also higher than Fe(II) and Fe(III) supported silica coagulants. The degradation mechanism was investigated for simulated nanofiltration concentrates, which suggested the Cys-Fe(III)@mSiO$_2$ Fenton/coagulation process might comprehensively reduce the color and COD for real nanofiltration concentrates effluent.

Keywords: Simulated nanofiltration concentrates; Dye wastewater; Silica microgel coagulant; Heterogeneous Fenton; Synthetic dyes

1. Introduction

Nanofiltration wastewater, containing highly complex mixtures of suspend solids, metal salts, auxiliary chemicals, dyes and other organic matters, not only pollutes the environment but also endangers human health due to its toxicity [1,2]. Therefore, the treatment of nanofiltration wastewater has become a hotspot in recent years. Photocatalytic processes [3–5], coagulation-flocculation processes [6–8], advanced oxidation processes (AOPs) [9–11] and so on, have been applied to the treatment of nanofiltration wastewater. In these processes, advanced oxidation process, especially the Fenton degradation, [12,13] due to its fast degradation rate and simple operation, has caused extensive research interest. However, the Fenton system also showed limitations during the degradation process,such as low operation pH range (normally 3-4), low cycle rate between Fe^{2+} and Fe^{3+} and low ·OH generation rate [14,15].

To overcome the problems of traditional Fenton process, the combined degradation process of Fenton, Fenton/

*Corresponding author.

coagulation for nanofiltration concentrates have raised great concern in recent years [22,23]. Ma et al. found that the flocs of single Fe^{3+} were small and loose which need a long time to set down. When the coagulation of polyaluminium chloride (PAC) was added, not only was the flocs setting time reduced, but the color and COD (chemical oxygen demand) removal of wastewater was improved [24]. Zhang et al. found high color (99%) and COD (80%) removal of the synthetic effluent could be realized by Fenton/coagulation (FC) processes [25]. Therefore, a combination of Fenton, Fenton-like degradation and silica coagulation(Fe(II)@mSiO$_2$, Fe(III)@mSiO$_2$,) methods might greatly enhance the degradation efficiencies for nanofiltration wastewater. The degradation of homogeneous Fenton-like degradation could be changed to heterogeneous Fenton one since iron ions are embedded and supported by the nano-size silica microgels, which could reduce the iron loading for the degradation systems and broaden the effective degradation pH. Since iron ions were positively charged, the surface of silica microgel was modified and the iron loading in these methods might be reduced since the combined coagulating effects of iron ions and silica microgel. For the composition of nanofiltration wastewater is complex and fluctuating, simulated model was established which contains four dyes (acid, basic and reactive dyes) and three anionic species (Cl^-, NO_3^-, SO_4^{2-}) in order to simplify the complexity of the system and to deeply investigate the removal mechanism [26]. In addition, L-cysteine (Cys), as a kind of sulfur-containing amino acid, was also added into above degradation systems, which could strengthen the conversion rate between Fe^{3+} and Fe^{2+} in aqueous solutions [19–21]. In this work, L-cysteine modified Fe^{3+} supported silica microgel (Cys-Fe(III)@mSiO$_2$) was also fabricated and the degradation efficiencies of four dyes were also discussed in a wide pH range. The reported results could add new understanding for Fenton, Fenton/coagulation degradation systems for actual highly polluted nanofiltration wastewater.

2. Experimental

2.1. Chemicals and materials

Four dyes (2 basic dyes, 1 reactive dye, 1 acid dye, purchased from Hefei Leung Biotechnology Co., LTD, China) and 3 common metal salts (NaCl, $NaNO_3$, Na_2SO_4, purchased from Tianjin Guangfu Chemical Reagent Co., LTD) were selected for preparing simulated nanofiltration concentrates of dye wastewater (SNDW). For simplicity, these dyes would be referred in the text as their corresponding code name shown in Table 1. The real field dye nanofiltration concentrates containing multiple synthetic dyes were sampled from a textile wastewater treatment plant of Jiangsu, China. The textile wastewater was treated with activated sludge process, clarified and nanofiltrated by thin film composite hollow fiber membrane with selective layer of crosslinked polyvinyl alcohol (PVA) and polyquaternium-10 on the outside of the support hollow fiber. In appearance, the concentrates sample look purple and have about 561 mg/L of COD, pH ~7.6 and 16252.5 mg/L of total dissolved solids (TDS). Sodium silicate (molar ratio: Na_2O:3.2SiO_2, 34 wt% SiO_2) was purchased from Shandong Dongyue Chemical Co. LTD. Ferrous sulfate heptahydrate ($FeSO_4 \cdot 7H_2O$), ferric sulfate ($Fe_2(SO_4)_3$), L-cysteine (Cys), hydrogen peroxide (H_2O_2, 30 wt%), concentrated sulfuric acid (H_2SO_4, 95–98 wt%), polyacrylamide (PAM, 1 wt‰) and lime ($Ca(OH)_2$, 10 wt%) were purchased from Tianjin Wind Ship Chemical Co. LTD. Sulfuric acid (H_2SO_4, 2.0 mol/L) and Hydrochloric acid (HCl, 2.0 mol/L) were applied to adjust the solution pH. All chemicals were of analytical grade.

2.2. Synthesis of mSiO$_2$, Fe(II)@mSiO$_2$, Fe(III)@mSiO$_2$ and Cys-Fe(III)@mSiO$_2$ for the degradation of nanofiltration concentrates

The mSiO$_2$, Fe(II)@mSiO$_2$, Fe(III)@mSiO$_2$ and Cys-Fe(III)@mSiO$_2$ were fabricated by polysilicate microgel method. A glass beaker equipped with 45 mL distilled water, placed on the magnetic stirrer to maintain rapidly mixing state at room temperature. And then 4.065 g of sodium silicate with certain amount of 2 mol/L H_2SO_4 solution were added in the beaker to get homogeneous polysilicate microgel solution which was mixed for 5 min at pH 9.12. Immediately after the pH was adjusted to the desired value with 95–98 wt% H_2SO_4 for getting the more stable polysilicate microgel solution, certain amount of ferric sulfate and L-cysteine were added to the above solution and stirred for 30 min to get the final Cys-Fe(III)@mSiO$_2$ Fenton/coagulation materials. Additionally, Fe(III)@mSiO$_2$ and Fe(II)@mSiO$_2$ Fenton/coagulation were also prepared as above without addition of L-cysteine. But for Fe(II)@mSiO$_2$Fenton/coagulation degradation system, the addition of ferric sulfate was replaced by ferrous sulfate heptahydrate. Finally, mSiO$_2$ was also prepared as above without the addition of L-cysteine and either kind of sulfate salts.

2.3. Fenton/coagulation experiments

The 1000 mg/L simulated nanofiltration concentrates of dye wastewater (SNDW) was prepared by dissolving 4 dyes (each dye dosage was 250 mg) and 3 common anions

Table 1
Characteristic of dyes for iron ion supported nano-size silica microgel Fenton/coagulation processes

Name of dyes	Code name	Type of dyes	Molecular formula	λ_{max}	Molecular weight (g/mol)
Methylene blue	MB	Basic dye	$C_{16}H_{18}ClN_3S$	664	374
Alcian blue 8GX	ABR	Basic dye	$C_{56}H_{68}C_{l4}CuN_{16}S_4$	611	1299
Remazol brilliant blue R	RBBR	Reactive dye	$C_{22}H_{16}N_2Na_2O_{11}S_3$	590	627
Brilliant blue R	BBRA	Acid dye	$C_{45}H_{44}N_3NaO_7S_2$	554	826

(1g Cl^-, 1g NO_3^-, 1g SO_4^{2-}) in 1.0 L distilled water. All Fenton/coagulation experiments were operated at room temperature and kept rapidly stirring at 200 r/min on the magnetic stirring. The degradation was triggered by adding required amount of Fenton/coagulation system and H_2O_2 dosages to 50 mL SNDW and the degradation time was 30 min, while before doing that the pH of the solution was adjusted to the desired value by adding 2 mol/L HCl. Then adding 10 wt% $Ca(OH)_2$ and 1 wt‰ polyacrylamide (PAM) to quench the degradation and accelerate flocculation process, respectively. After degradation of Fenton/coagulation system,the portion of supernatant was taken to measure color and COD. All the experiments were repeated three times under certain conditions. Similarly, the real field dye nanofiltration concentrates were also degraded with the same method. The color removal value was the average of the four dyes.

2.4. Characterizations

The samples of $mSiO_2$, Fe(II)@$mSiO_2$, Fe(III)@$mSiO_2$ and Cys-Fe(III)@$mSiO_2$ were placed in beakers and dried in a vacuum drying oven at 105°C for 12 h to get solid state samples. And then the mortar was used to grind the solid samples for the characterizations of SEM, TEM, FT-IR, XRD and thermogravimetric analysis (TGA). The field emission scanning electron microscopy (SEM, Hitachi, S-4800) images and the high resolution transmission electron microscopy (HRTEM, Hitachi, H-7650) images were obtained to study the morphology of these degradation systems. Fourier transform infrared spectra (FT-IR) were measured using a Bruker TENSOR37 FT-IR spectrometer. The samples were evenly grinded and pressed into tablets with KBr for the measurement. In order to analyze the crystallinity of these materials, X-ray powder diffraction (XRD) was carried out on a Bruker D8 Advance X-ray diffractometer using Cu Kα radiation as the X-ray source. Thermogravimetric analysis (TGA) were performed by using a STA 409 PC thermal analyzer (NETZSCH, Germany) in air with heating rate of 5°C/min from ambient temperature to 800°C.

2.5. Chemical analysis

Prior to or after treatment,the clear liquid samples of sampling to determine the COD and color removal of the SNDW.COD was determined with COD-571 meter (ShangHai HuaYuan, China). The wavelength of 554, 590, 611 and 664 nm are the maximum absorption wavelength of Brilliant blue R, Remazol brilliant blue R, Alcian blue 8GX, Methylene blue, respectively. With scanning the sample by UV-vis spectrophotometer(Rex 752, ShangHai, China), the UV-vis integral has linear relationship with dye concentrations when the nanofiltration concentrates was diluted for certain times (integrated range: 350~650 nm). Therefore, the color value of each sample was measured at its highest absorption peak for the four dyes of 554, 590, 611 and 664 nm (view Table 1). The pH was measured using portable pH meter (pHS-3C, China). The initial color and COD of the nanofiltration wastewater were determined after the wastewater was diluted to certain ratio with deionized water.

3. Results and discussion

3.1. Structural characterizations

Fig. 1 shows the SEM and TEM images of $mSiO_2$, Fe(II)@$mSiO_2$, Fe(III)@$mSiO_2$ and Cys-Fe(III)@$mSiO_2$.The $mSiO_2$ (Fig. 1A) was made up of large block particles or plate-like structures with the average particle size of approximately 3.0–6.0 μm in diameter. The large block particles structures were also identified in the TEM (Fig. 1B). When the iron ions were added, the structures of Fe(II)@$mSiO_2$ (Fig. 1C) and Fe(III)@$mSiO_2$ (Fig. 1E) become dispersed and the particle size was reduced, which implied the cross-copolymerization formed between Fe and Si in dried coagulants [27]. The results could also be evidenced clearly from TEM image (Fig. 1D) and FT-IR characterization (Fig. 2). The Cys-Fe(III)@$mSiO_2$ (Fig. 1G) particles showed a more uniform crosslinked morphology and dispersed structure when the L-cysteine was added. Meanwhile, Fe(II)@$mSiO_2$ (Fig. 1C) and Fe(III)@$mSiO_2$ (Fig. 1E) had fewer branch-like than Cys-Fe(III)@$mSiO_2$ (Fig. 1G), which implies the Cys could strengthen the cross-copolymerization between Fe and Si complexes. In addition, less-branched coagulants were less favorable than multi-branched and fractal dimension ones [28]. The compact gel morphology of solid Cys-Fe(III)@$mSiO_2$ (Fig. 1G) showed high polymerization degree to coagulant colloidal particles and formed more bridge-aggregated network during the waste water treatment systems. The TEM images of Fe(II)@$mSiO_2$, Fe(III)@$mSiO_2$ and Cys-Fe(III)@$mSiO_2$ proved the similar results (Fig. 1B, 1D, 1F). The diameter distribution was relatively uniform, which could be also beneficial to improve the dissolution and coagulation abilities of the Fenton/coagulation system.

As shown in Fig. 2, the FT-IR spectra of four degradation systems exhibited a broad absorption peak in the range of 1640–1670 cm^{-1}, which could be associated with the stretching vibration of –OH and the bending vibration of water absorbed, polymerized and crystallized in above degradation systems [29,30]. Meanwhile, the absorption peaks at 1750 cm^{-1}, which were attributed to the CO_2 among the around atmosphere [31]. The peaks at 790–800 cm^{-1} and 1380 cm^{-1} assigned to the connection of Si-O-Si bonds and Si-O bonds respectively [32]. These absorption peaks did not present in the spectra of other three coagulants, which suggested the structures of $mSiO_2$ were changed after the modification of $FeSO_4$, $Fe_2(SO_4)_3$ and Cys, respectively. Meanwhile there were strong absorption peaks at 1095–1130 cm^{-1} that could be contributed to the stretching vibration of Fe-O-Fe bonds [33]. While, these peaks around 1160 cm^{-1} corresponded to the asymmetric stretching vibration of Fe-O-Fe bonds. Furthermore, the peaks at 460–650 cm^{-1} were related to the bending vibration of Fe-OH bonds and the winding vibration of Fe-O, Si-O bonds [30]. However, the peak around 640 cm^{-1} disappeared after the addition of Cys, which implied the existence of cross-copolymerization of Fe(III) and Cys hydroxyl polymers in the coagulant. Additionally, Cys-Fe(III)@$mSiO_2$ also exhibited the characteristic peaks at 970–1010 cm^{-1}, which were attributed to the bending vibration of Si-O-Fe bonds [27]. All of these data confirmed the Fe(II)@$mSiO_2$, Fe(III)@$mSiO_2$ and Cys-Fe(III)@$mSiO_2$ were not a simple mixture of raw materials. New chemical compounds consisting of iron and silica were formed, which also could be confirmed with the XRD analysis.

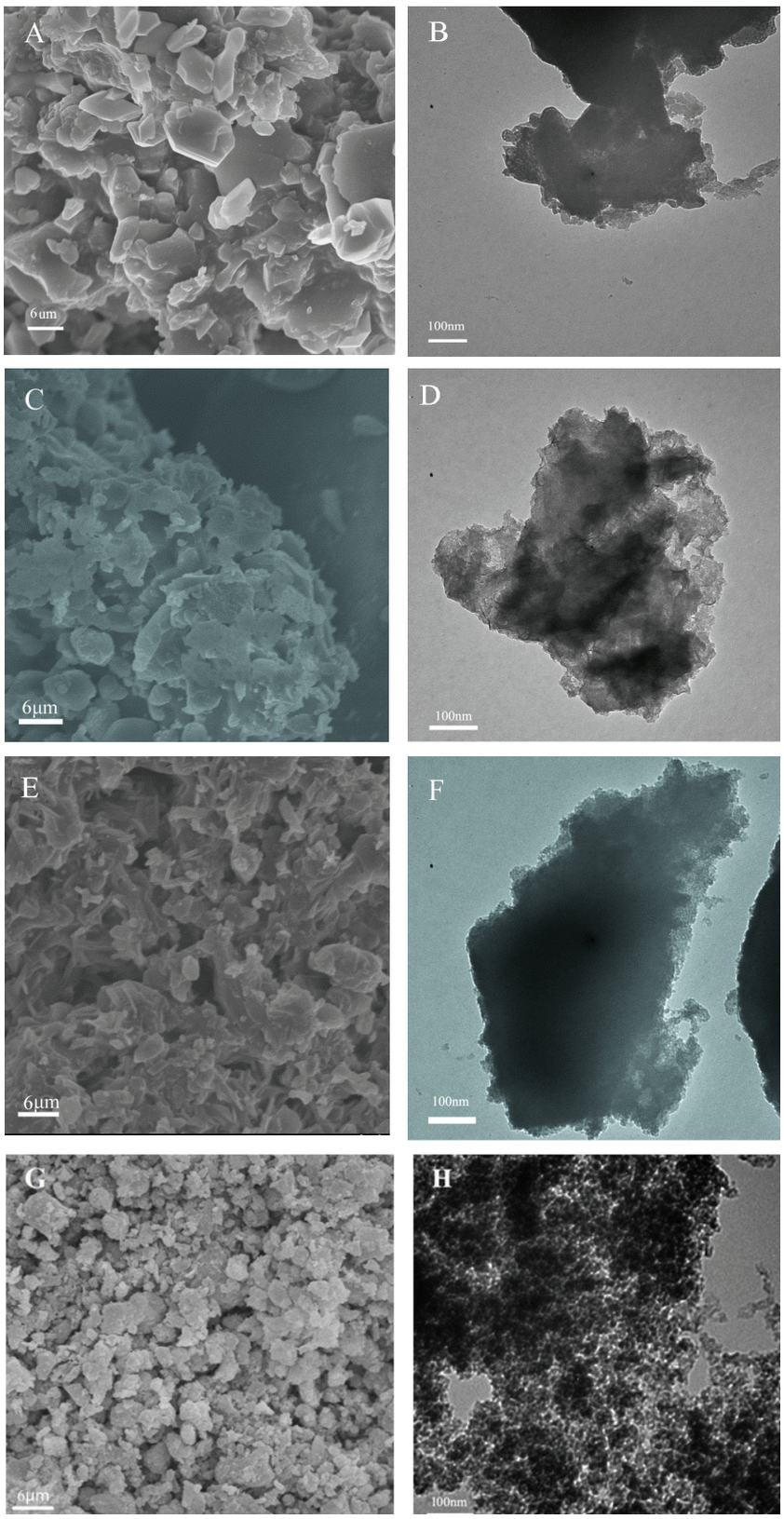

Fig.1. SEM and TEM images of $mSiO_2$ (A and B), Fe(II)@$mSiO_2$ (C and D), Fe(III)@$mSiO_2$ (E and F), Cys-Fe(III)@$mSiO_2$ (G and H).

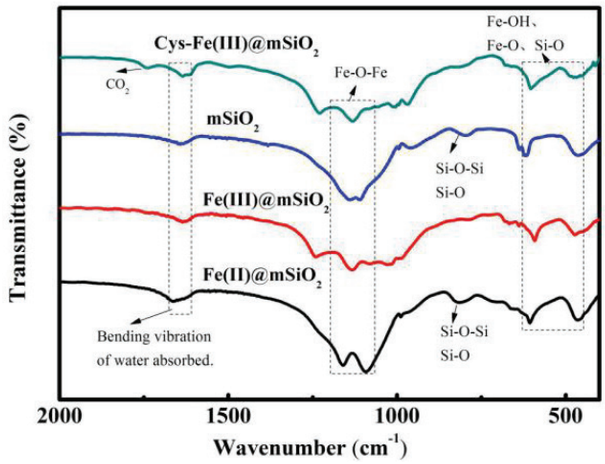

Fig. 2. FT-IR spectra of $mSiO_2$, Fe(II)@$mSiO_2$, Fe(III)@$mSiO_2$ and Cys-Fe(III)@$mSiO_2$.

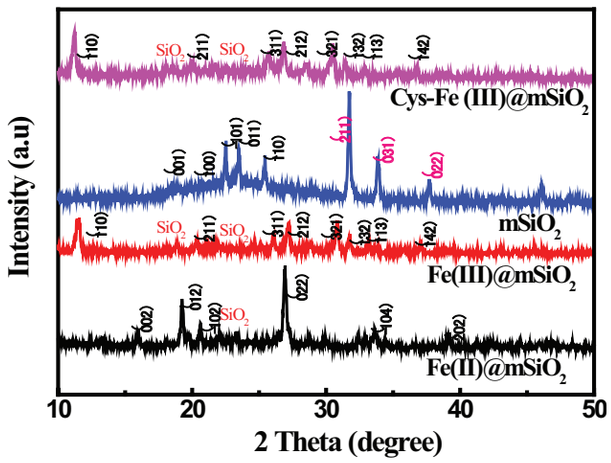

Fig. 3. XRD spectra of $mSiO_2$, Fe(II)@$mSiO_2$, Fe(III)@$mSiO_2$ and Cys-Fe(III)@$mSiO_2$.

The XRD spectra of $mSiO_2$, Fe(II)@$mSiO_2$, Fe(III)@$mSiO_2$ and Cys-Fe(III)@$mSiO_2$ are shown in Fig. 3. Every curve showed obviously diffractive peaks. From Fig. 3, it can be seen that $mSiO_2$ consists of pure silica. The sharp peaks of diffraction at 18.5°, 20.64°, 22.52°, 23.46° and 25.44° occurred in the spectrogram of pure SiO_2 (JCPDS No.82-1571) and the diffraction peaks at 31.76°, 33.84°, 37.7°, 46.06°, 48.18° corresponds to the Na_2SO_4 crystal (JCPDS No.24-1132) [34], it is different from Fe(III)@$mSiO_2$ and Fe(II)@$mSiO_2$. These phenomena indicated the different valences of iron ions and silicon are polymerized to some new compounds rather than the simple mixture of the raw materials [28]. The sharp diffraction peaks of Fe(II)@$mSiO_2$ at 2θ = 16°, 19.24°, 20.62°, 26.94°, 33.62° and 39.18° occurred in the spectrogram of $Na_2Fe(SO_4)24H_2O$ crystal (JCPDS No.25-0837). But the peaks of diffraction disappeared completely at the same diffraction angle in the spectrogram of Fe(III)@$mSiO_2$ curves, and the 2θ values at 11.56°, 20.3°, 26.08°, 27.22°, 30.86°, 31.78°, 33.2° and 37.04° could be indexed to the (110), (121), (311), (212), (231), (132), (113) and (142) planes of Fe(III) ($Na_3Fe(SO_4)_3{\cdot}3H_2O$, JCPDS No.71-1839). These results proved the different valences of iron ions had some effects on the polymerization and conformation of the two coagulants [29]. The diffraction peak of Cys-Fe(III)@$mSiO_2$ at 11.26°, 20.08°, 25.72°, 26.86° and 30.5° is equivalent to $Na_3Fe(SO_4)_3{\cdot}H_2O$ (JCPDS No.16-0937), which implied the existence of cross-copolymerization of Fe(III) and Cys polymers in coagulant. This is also consistent with FT-IR analysis.

Thermogravimetric analysis (TGA) of silica-based samples is shown in Fig. 4. As shown in Fig. 4, TGA curve of $mSiO_2$ showed one weight loss stage. The weight loss stage from the indoor temperature to 92°C ($mSiO_2$) corresponded to the water loss of the sample, which showed a weight loss of 15.04 % in this range and could get high silicon content of the residue. The weight loss stage from the ambient temperature to the 112°C (Fe(II)@$mSiO_2$) and 111°C (Fe(III)@$mSiO_2$) corresponded to the dehydration of coagulants, while the weight loss stage at 112–201°C (Fe(II)@$mSiO_2$) and 120–175°C (Fe(III)@$mSiO_2$) corresponded to the surface hydroxyl group loss of the coagulants, and the weight loss stage at 500–640°C

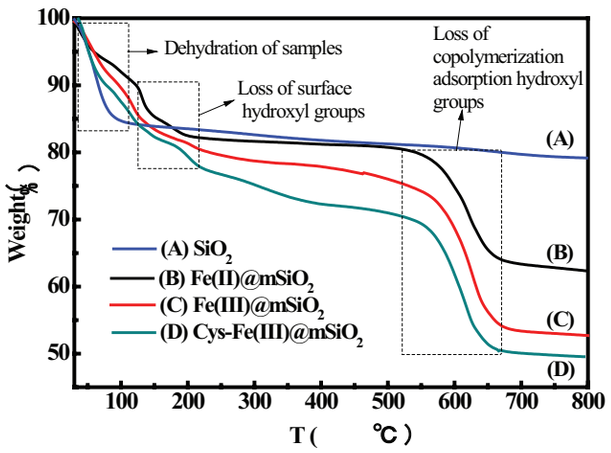

Fig. 4. TGA spectra of $mSiO_2$, Fe(II)@$mSiO_2$, Fe(III)@$mSiO_2$ and Cys-Fe(III)@$mSiO_2$.

(Fe(II)@$mSiO_2$) and 550–680°C (Fe(III)@$mSiO_2$) corresponded the cross-copolymerization adsorption of these coagulants. These phenomena indicated the cross-copolymerization constructions of the latter one was more complex than the former one and the latter had more surface hydroxyl groups which were obviously appeared on the thermal TGA curves. Generally speaking, the TGA curve of the Cys-Fe(III)@$mSiO_2$ was similar to the Fe(III)@$mSiO_2$. But the weight loss of Cys-Fe(III)@$mSiO_2$ (9.76%) was also higher than that of Fe(III)@$mSiO_2$ (7.54%), which was probably due to the decomposition of extra Cys and ligands between Cys and iron ions. Meanwhile, the rate of water loss for Cys-Fe(III)@$mSiO_2$ system was also faster than that of the other systems which indicates the synthesis had enhanced the porosity of Cys-Fe(III)@$mSiO_2$. This property could make the coagulant remove the moisture easily. Finally, the TGA curve of Cys-Fe(III)@$mSiO_2$ became stable at approximately 700°C, which was higher than other three systems. It could be affirmed the ligands between Cys and metal ions significantly changed the decomposition temperature and thermal stability for Cys-Fe(III)@$mSiO_2$.

3.2. Iron ions concentration effect

Fig. 5 presents the iron ions concentration changes for the Fe(II)@mSiO$_2$, Fe(III)@mSiO$_2$ and Cys-Fe(III)@mSiO$_2$ heterogeneous Fenton/coagulation systems on the color and COD removal efficiencies for the simulated nanofiltration concentrates. Fig. 5a, Fig. 5b and Fig. 5c indicate all of above Fenton/coagulation systems achieved higher color removal efficiencies for the MB and ABR colorants than other two dyes. The results showed the basic dyes (MB and ABR) are more easily to be degraded by the Fenton/coagulation systems while the reactive dye (RBBR) and acid dye (BBRA) are more refractory. For all the concentration changes of the iron ions, color removal would be faster in the first 50–100 mg/L. Fig. 5a and Fig. 5b also show that the optimal dosage of iron concentration is 100 mg/L. When below or above this value, the color removal efficiency would be reduced for Fe(II)@mSiO$_2$ and Fe(III)@mSiO$_2$. Especially for the ion concentration in the range of 50–100 mg/L, the color removal efficiency of the Fe(II)@mSiO$_2$ is higher than that of the Fe(III)@mSiO$_2$. But the reversed result for the degradation efficiency was obtained when the practical quantity was in the range of 100–230 mg/L, which might be due to Fe(II) are more active than Fe(III) to activate H_2O_2 for generating highly active ·OH and trigger free radical chain reactions[7]. However, with the Fe(III) dosage increasing of the Cys-Fe(III)@mSiO$_2$ at 50–230 mg/L, the color removal efficiencies of the simulated dyes continued to increase until the treated effluent turned to a clear state (such as Fig. 5c). As the exists of the Cys reducing sulfhydryl group, Cys could reduce the Fe^{3+} to Fe^{2+} with enhanced rate. Meanwhile, the Cys could form complexes with Fe^{3+}, which could reduce the precipitation of Fe^{3+} (Cys-Fe^{3+} complexes) [21,35]. On the other hand, Cys-Fe^{3+} complexes could increase the transformation rate from Fe^{3+} to Fe^{2+} by an internal redox triggered by protonation [23,36]. Fig. 5d indicates that the COD removal was a little lower for the Fe(II)@mSiO$_2$ than the other two iron silicon-based systems. The Fe(III) degradation systems had the similar treatment efficiencies and 80.75% COD were removed for Fe(III)@mSiO$_2$ at the optimal dosage of 150 mg/L. The Cys as the residual organic ligands might also increase the extra chemical oxygen demand for the wastewater treatment.

3.3. H_2O_2 concentration effect

H_2O_2 play an important role as an oxidant in the Fenton/coagulation degradation for generating the ·OH. To optimize the dose of H_2O_2 for the degradation, the molar ratio of H_2O_2 to iron ions was investigated at initial pH_0 =

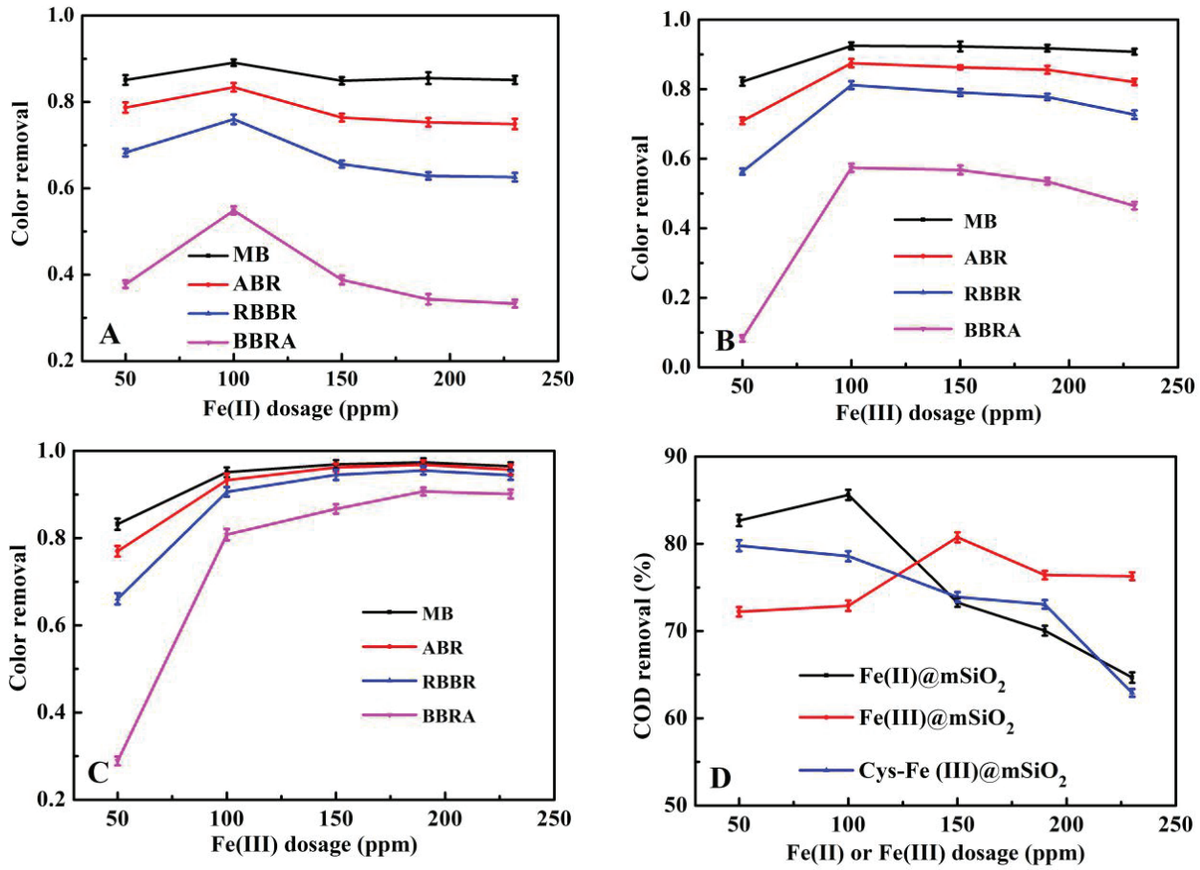

Fig. 5. Effect of iron ions concentration for Fe(II)@mSiO$_2$(a), Fe(III)@mSiO$_2$(b), Cys-Fe(III)@mSiO$_2$(c) on color removal and COD removal (d) during the degradation of Fenton/coagulation systems (30 min degradation time, pH_0 = 3 and the molar ratio of iron ions to H_2O_2 is 1:20).

3. Fig. 6 shows the removal of color and COD at different-molar ratio for the Fe(II)@mSiO$_2$, Fe(III)@mSiO$_2$ and Cys-Fe(III)@mSiO$_2$. The color and COD of the four dyes were obviously decreased when the molar ratio of H_2O_2 to iron increased for the Fe(II)@mSiO$_2$. The results indicated a progressive decrease in removal efficiency of the COD with the increase of oxidants. With the increasing of the molar ratio of H_2O_2 to Fe(III) from 10:1 to 20:1 for Fe(III)@mSiO$_2$, the COD removal of the effluent increased from 69.12 % to 80.75. When further increasing the molar ratio from 20:1 to 40:1, the COD removal decreased from 80.75% to 64.87% and the color removal of all dyes slightly decreased during all period from 10:1 to 40:1. Fe(III)@mSiO$_2$ maintained relatively higher and more stable color removal efficiency than Fe(II)@mSiO$_2$. And the opposite effect appeared for the COD removal, which indicates Fe(III)@mSiO$_2$ produced more colorless and organic intermediates and generate relatively higher COD value. From Fig. 6c and Fig. 6d, the color and COD could be almost removed from 10:1 to 40:1 for the Cys-Fe(III)@mSiO$_2$ since the proper H_2O_2 concentration for producing more ·OH and large amount of ferric hydroxo complexes generated by the redox reaction [37]. When the amount of hydrogen peroxide is changed, basic dyes are still the most easily to be degraded by the Fenton/coagulation systems. This phenomenon is similar to the results obtained from the change of the iron ion concentration. However, the COD removal decreased from 73.83 % to 55.05% when molar ratio was higher than 20:1, which might be due to the redundant H_2O_2 which would scavenge the ·OH. The regeneration of Fe^{2+} in the solution could be decreased. Meanwhile, redundant H_2O_2 would produce much more H^+ which could break the Cys-Fe(III) complexes, led to the decrease of the COD removal [38].

3.4. Initial degradation pH effect

Fig. 7 Effect of initial degradation pH for Fe(II)@mSiO$_2$ (a), Fe(III)@mSiO$_2$ (b), Cys-Fe(III)@mSiO$_2$ (c) on color removal and COD removal (d) during the degradation of Fenton/coagulation systems (150 mg/L iron ions, 30 min degradation time and the molar ratio of iron to H_2O_2 is 1:20).

Fig. 7 illustrates the effects of the initial degradation pH on color and COD removal for Fe(II)@mSiO$_2$, Fe(III)@mSiO$_2$ and Cys-Fe(III)@mSiO$_2$. The initial pH of the solution influences the Fenton oxidation efficiencies significantly [39,40]. The basic dyes are still the most easily degraded during the experiment pH range. From Fig. 7a, with the increasing of degradation pH from 2 to 3, the color and COD removal of Fe(II)@mSiO$_2$ were higher than those of Fe(III)@mSiO$_2$, especially in slightly acidic pH conditions. The formed flocs were large and dense and they could be easily precipitated at the experiment pH. The high color removal efficiencies for Cys-Fe(III)@mSiO$_2$ could be obtained at relatively wide pH range of 3 to 6.2. The degradation of BBRA color was more difficult, which varied from 80 % to 70.5 % at the pH of 3 to

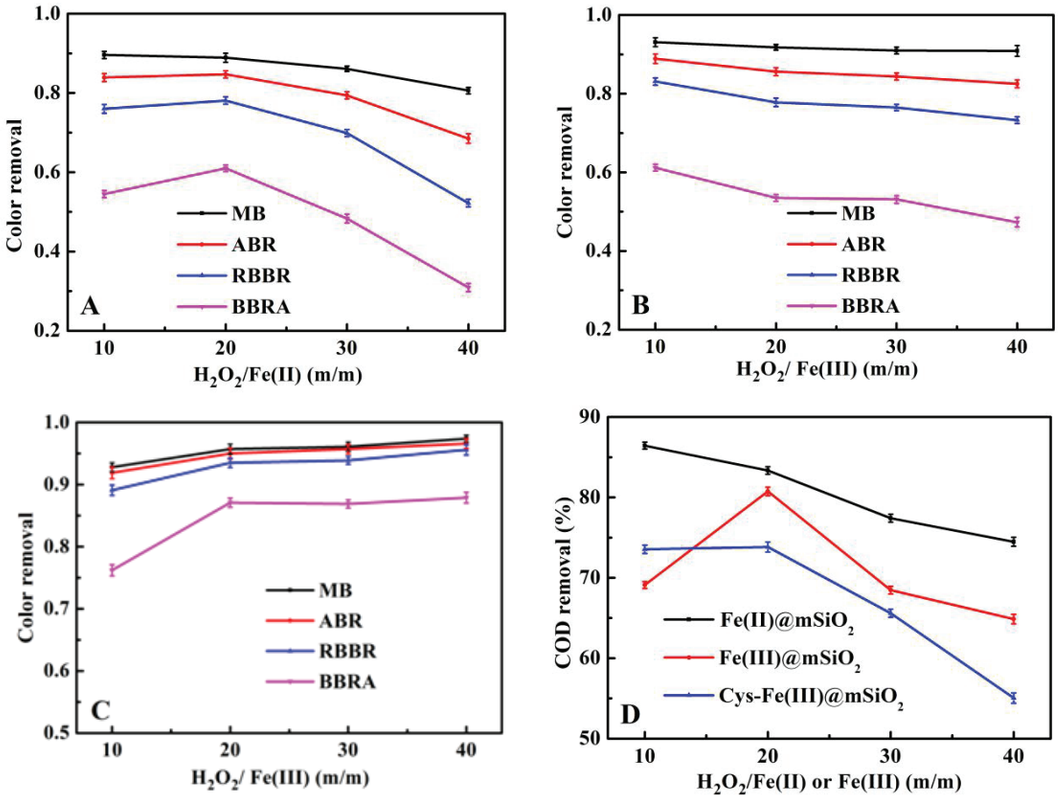

Fig. 6. Effect of H_2O_2 concentration for Fe(II)@mSiO$_2$ (a), Fe(III)@mSiO$_2$ (b), Cys-Fe(III)@mSiO$_2$ (c) on color removal and COD removal (d) during the degradation of Fenton/coagulation systems (150 mg/L iron ions, 30 min degradation time and pH_0 = 3).

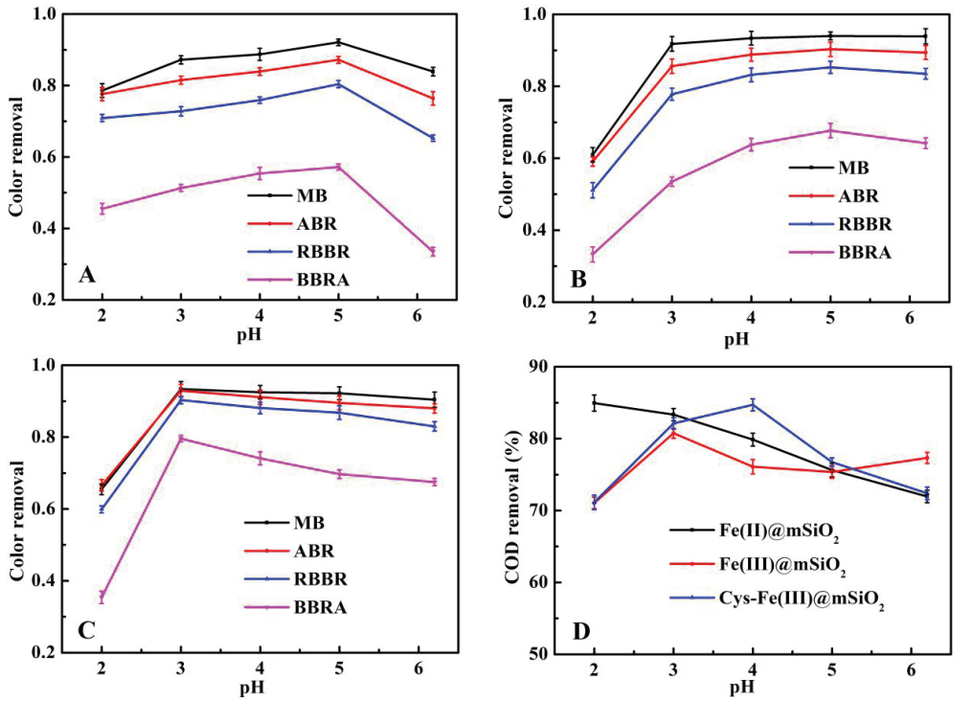

Fig. 7. Effect of initial degradation pH for Fe(II)@mSiO$_2$ (A), Fe(III)@mSiO$_2$ (B), Cys-Fe(III)@mSiO$_2$ (C) on color removal and COD removal (D) during the degradation of Fenton-like/coagulation systems (150 mg/L iron ions, 30 min degradation time and the molar ratio of iron to H_2O_2 is 1:20).

6.2. From Fig. 7d, the highest COD removal was 84.7 % at pH = 4. The color and COD removal of Cys-Fe(III)@mSiO$_2$ were less sensitive to pH variation, which was due to the higher stabilization and bridging, sweep capacity of the coagulant at all experimental pH values [21].

3.5. Degradation time effect

Fig. 8 shows the effect of degradation time on the color and COD removal for the Fe(II)@mSiO$_2$, Fe(III)@mSiO$_2$ and Cys-Fe(III)@mSiO$_2$ during the Fenton/coagulation degradation processes. Similarly, for all the degradation time, the basic dyes were still the most easily degraded. There appeared to be no obvious difference in color removal for the Fe(II)@mSiO$_2$ and Fe(III)@mSiO$_2$. In addition, 78.2 % color of the BBRA was removed at a short degradation time for 30 min. The color removal remained unchanged for prolonging the degradation time for the Cys-Fe(III)@mSiO$_2$, which showed the superior degradation rates compared with the former two degradation systems. From Fig. 8d, 81 % COD removal could be achieved at 15 min for the Fe(II)@mSiO$_2$. With the increasing of degradation time from 15 to 60 min, the COD removal increased slightly to 84%. In contrast, the efficiency of COD removal was only 60% at 15 min and 81% at 30 min for the Fe(III)@mSiO$_2$. Furthermore, 82.12% COD removal was achieved for the Cys-Fe(III)@mSiO$_2$ at the optional degradation of 30 min, which would be caused not only by the intermediates of the dyes but the residual Cys.

3.6. Setting time effect

In addition to the high settling velocity, high stabilization of the coagulation/flocculation flocculant agglomerates were also a prerequisite for an effective coagulation process. Fig. 9 discusses the influence of the precipitation setting time for the Fe(II)@mSiO$_2$, Fe(III)@mSiO$_2$ and Cys-Fe(III)@mSiO$_2$ on color and COD removal after the degradation of Fenton-like systems. As shown in Fig. 9, the decolorization efficiencies of the Fe(II)@mSiO$_2$ and Cys-Fe(III)@mSiO$_2$ were relatively higher than Fe(III)@mSiO$_2$, which showed a high stability during the same precipitation static time. Meanwhile, the color removal efficiency after the degradation of Cys-Fe(III)@mSiO$_2$ was highest among the three systems. With the increase of the settling time, the removal efficiencies of the color and COD decreased sharply for Fe(II)@mSiO$_2$ and Fe(III)@mSiO$_2$, which shows the agglomerates of these systems are less stable than that of Cys-Fe(III)@mSiO$_2$.The COD removal showed a relatively stable and even slightly increased state for the Cys-Fe(III)@mSiO$_2$, which might be due to the disappearance of the hydrogen peroxide and the dissolved Cys as the residual organic ligands increased the extra chemical oxygen demand.

3.7. Degradation efficiencies for the real field nanofiltration concentrates and the proposed degradation mechanism

In order to compare and clarify the color removal and COD degradation differences of simulated and real field dye nanofiltration concentrates, the degradation performance of real field dye nanofiltration concentrates in differ-

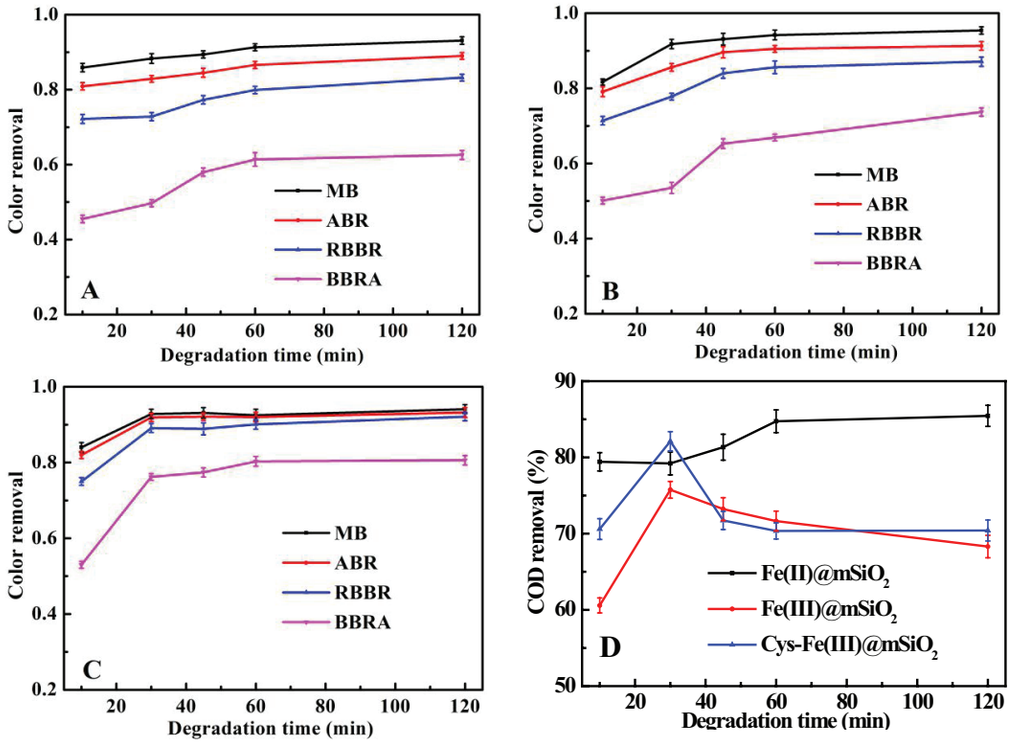

Fig. 8. Effect of degradation time for Fe(II)@mSiO$_2$ (a), Fe(III)@mSiO$_2$ (b), Cys-Fe(III)@mSiO$_2$ (c) on color removal and COD removal (d) during the degradation of Fenton/coagulation systems (150 mg/L iron ions, pH$_0$ = 3, the molar ratio of iron to H_2O_2 is 1:20).

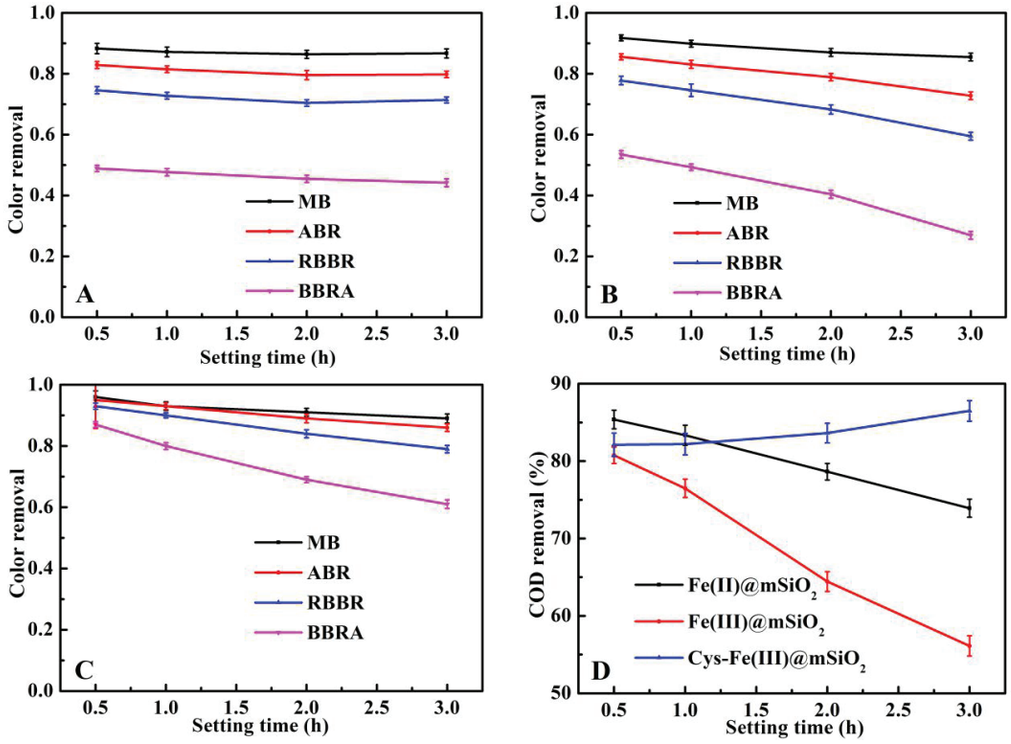

Fig. 9. Effect of setting time for Fe(II)@mSiO$_2$ (a), Fe(III)@mSiO$_2$ (b), Cys-Fe(III)@mSiO$_2$ (c) on color removal and COD removal (d) after the degradation of Fenton/coagulation systems (150 mg/L iron ions, 30 min degradation time, pH$_0$ = 3 and the molar ratio of iron to H_2O_2 is 1: 20).

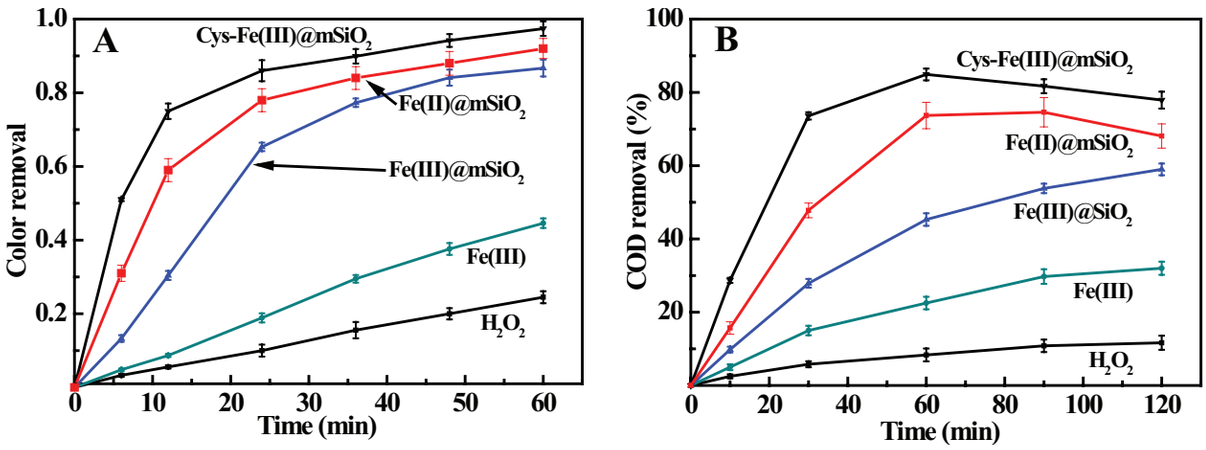

Fig. 10. Color removal efficiencies of real field dye nanofiltration concentrates (a) and COD (b) in different Fe(III) Fenton/coagulation systems (150 mg/L iron ions, 30 min degradation time, pH_0= 3 and the molar ratio of iron to H_2O_2 is 1:20).

ent Fe(III) Fenton/coagulation systems are investigated and related results are shown in Fig. 10. In Fig. 10, the degradation efficiency of color could be neglected under pure H_2O_2 conditions. About 40% color and 20% COD were removed in the pure Fe(III)/H_2O_2 degradation system, which was higher than those of pure H_2O_2. More than 90% colored dyes and 60% COD removed for Fe(III)@$mSiO_2$/H_2O_2 system. Moreover, the addition of Cys into the Fe(III)@$mSiO_2$ (Cys-Fe(III)@$mSiO_2$/H_2O_2) significantly enhanced the color removal and COD degradation of real nanofiltration concentrates. More than 95% colored dyes and 80% COD were removed under the same degradation conditions. Hence, the color and COD removal were significantly higher than those of pure H_2O_2 and pure Fe(III)/H_2O_2 degradation system when the combination of Fenton/coagulation systems was used to treat the actual nanofiltration wastewater. The color and COD removal efficiencies of the real field dye nanofiltration concentrates showed the similar trends with those of the simulated nanofiltration concentrates of dye wastewater by Fe(II)@$mSiO_2$/H_2O_2 system. The COD removal efficiencies of the Fe(II)@$mSiO_2$/H_2O_2 system decreased after 90 min, which might be due to the loose structure of the agglomerates and re-dissolve of the precipitates. A little higher treatment efficiency by the Cys-Fe(III)@$mSiO_2$/H_2O_2 system was also achieved for the simulated and the real field nanofiltration concentrates. These could conclude the Fe(III)@$mSiO_2$/H_2O_2 system degraded the colored dye in the nanofiltration wastewater into a colorless intermediate product. And the addition of Cys into above degradation system reduced the production of intermediates more effectively [21,41].

For homogeneous Fenton degradation, the iron ions (both the Fe(III) and Fe(II) ions) cannot show efficient degradation and the flocs of iron ions are small and loose, which cannot get clear and transparent supernatant for nanofiltration concentrates of dye wastewater. After Fe(III) was coated on the surface of nano-size silica microgel, the Fenton degradation of these iron ions could be changed from homogeneous Fenton to heterogeneous Fenton degradation for the nanofiltration concentrates. The iron loading for the degradation systems could be reduced and the effective degradation pH could be broadened, which also were evidenced by other investigation results [21]. The heterogeneous Fenton degradation could greatly reduce the iron loading and usage in degradation processes. Hence, the reduced iron ions on the surface of Fe(III)@$mSiO_2$ could show broadened pH usage condition in acid and near neutral pH condition (2~6.5) for heterogeneous Fenton degradation and enhanced coagulation efficiency with less iron sludge.

Besides, for the Cys-Fe(III)@$mSiO_2$ degradation system, L-cysteine (Cys) could form complexes with Fe(III) ions and then reduce Fe(III) to Fe(II) for its reducing sulfhydryl group (–SH) [41]. These complexes on the surface of Cys-Fe(III)@$mSiO_2$ reduced the precipitation of Fe(III) and unexpectedly enhanced the Fenton oxidation activities for nanofiltration concentrates of dye wastewater. The Fenton degradation efficiencies were further enhanced with Fe(III) ions on the surface of silica microgel. The reduced iron ions on the surface of Fe(III)@$mSiO_2$ could show broadened pH usage condition in acid and near neutral pH condition (2~6.5) for heterogeneous Fenton degradation and enhanced coagulation efficiency with less iron sludge, which the processes are simple and cost-effective. Hence, the Cys-Fe(III)@$mSiO_2$ degradation for nanofiltration concentrates have much more advantages compared with common iron ions system.

4. Conclusions

In this study, different three kinds of nano silica microgel Fenton/coagulation (Fe(II)@$mSiO_2$, Fe(III)@$mSiO_2$ and Cys-Fe(III)@$mSiO_2$) degradation systems for simulated nanofiltration concentrates of dye wastewater were systematically investigated. With SEM, TEM, XRD and other characterizations, the cross-copolymerization formed between Fe and Si in three different dried coagulants and the incorporation of L-cysteine enhances the cross-linking copolymerization between Fe and Si complexes, which is important for degradation of color and COD. The addition of L-cysteine to the Fe(III)@$mSiO_2$ system showed the highest degradation efficiencies for wastewater (95% color and 80% COD) since L-cysteine could reduce the Fe^{3+} ions to Fe^{2+} under highly concentrated anionic ions (Cl^-, NO^{3-}, SO_4^{2-}),

which broadened the range of initial degradation pH even under a relatively low iron ions concentration. Cys-Fe(III)@$mSiO_2$ degradation system also showed a relative higher adsorption and coagulation capacity compared with other two Fe(II)@$mSiO_2$, Fe(III)@$mSiO_2$ degradation systems for prolong the precipitation setting time from 0.5 h to 3 h. The degradation of two basic dyes (MB and ABR) is the highest and acid dye (BBRA) is the most difficult to be degraded among all the above dyes. Unlike the degradation of the Fe(II)@$mSiO_2$ and Fe(III)@$mSiO_2$, the COD removal of Cys-Fe(III)@$mSiO_2$ rose remarkably which could open up an inspiring research for actual nanofiltration concentrates of dye wastewater.

Acknowledgments

This work was supported by the National Natural Science Foundation of China (51472179, 51572192, 51772205 and 51772208), General Program of Municipal Natural Science Foundation of Tianjin (17JCYBJC17000 and 17JCYBJC22700). The authors declare that they have no conflict of interest.

References

[1] J. Zhang, S. Chen, Y. Zhang, X. Quan, H.M. Zhao, Y.B. Zhang, Reduction of acute toxicity and genotoxicity of dye effluent using Fenton-coagulation process, J. Hazard. Mater., 274 (2014) 198–204.

[2] C.Z. Sun, Q.Y. Yue, B.Y. Gao, B.C. Cao, R.M. Mu, Synthesis and floc properties of polymeric ferric aluminum chloride-polydimethyl diallylammonium chloride coagulant in coagulating humic acid-kaolin synthetic water, Chem. Eng. J., 185 (2012) 29–34.

[3] H. Park, H.I. Kim, G.H. Moon, W. Choi, Photoinduced charge transfer processes in solar photocatalysis based on modified TiO_2, Energ. Environ. Sci., 9 (2016) 411–433.

[4] L.Q. Ye, Y.R. Su, X.L. Jin, H.Q. Xie, C. Zhang, Recent advances in BiOX (X= Cl, Br and I) photocatalysts: synthesis, modification, facet effects and mechanisms, Environ. Sci. Nano., 1 (2014) 90–112.

[5] C.Y. Wang, X. Zhang, H.B. Qiu, W.K. Wang, G.X. Huang, Photocatalytic degradation of bisphenol A byoxygen-rich and highly visible-light responsive $Bi_{12}O_{17}C_{12}$ nanobelts, Appl. Catal. B-Environ., 200 (2017) 659–665.

[6] J.Y. Li, L. Zhao, L.L. Qin, X.J. Tian, A.M. Wang, Removal of refractory organics in nanofiltration concentrates of municipal solid waste leachate treatment plants by combined Fenton-oxidative-coagulation with photo-Fenton processes, Chemosphere, 146 (2016) 442–449.

[7] L.F. Guerreiro, C.S. Rodrigues, R.M. Duda, R.A. de Oliveira, R.A. Boaventura, Treatment of sugarcane vinasse by combination of coagulation/flocculation and Fenton's oxidation, J. Environ. Manage., 181 (2016) 237–248.

[8] Y.F. Wang, K.F. Chen, L.H. Mo, J. Li, J. Xu, Optimization of coagulation-flocculation process for paper making-reconstituted tobacco slice wastewater treatment using response surface methodology, J. Ind. Eng. Chem., 20 (2014) 391–396.

[9] S. Giannakis, M. Jovic, N. Gasilova, M.P. Gelabert, S. Schindelholz, Iohexol degradation in wastewater and urine by UV-based Advanced Oxidation Processes (AOPs): Process modeling and by-products identification, J. Environ. Manage., 195 (2017) 174–185.

[10] C. Amor, E.D. Torres-Socías, J.A. Peres, M.I. Maldonado, Mature landfill leachate treatment by coagulation/flocculation combined with Fenton and solar photo-Fenton processes, J. Hazard. Mater., 286 (2015) 261–268.

[11] A.J. Expósito, J.M. Monteagudo, A. Durán, A. Fernandez, Dynamic behavior of hydroxyl radical in sono-photo-Fenton mineralization of synthetic municipal wastewater effluent containing antipyrine, Ultraso. Sonochem., 35 (2017) 185–195.

[12] J. Bolobajev, E. Kattel, M. Viisimaa, A. Goi, M. Trapido, Reuse of ferric sludge as an iron source for the Fenton-based process in wastewater treatment, Chem. Eng. J., 255 (2014) 8–13.

[13] J. Rodríguez-Chueca, C. Amor, J.R. Fernandes, P.B. Tavares, M.S. Lucas, Treatment of crystallized-fruit wastewater by UV-A LED photo-Fenton and coagulation-flocculation, Chemosphere, 145 (2016)351–359.

[14] R.X. Huang, Z.Q. Fang, X.M. Yan, W. Cheng, Heterogeneous sono-Fenton catalytic degradation of bisphenol A by Fe_3O_4 magnetic nanoparticles under neutral condition, Chem. Eng. J., 197 (2012) 242–249.

[15] C.K. Wang, Y.H. Shih, Degradation and detoxification of diazinon by sono-Fenton and sono-Fenton-like processes, Sep. Purif. Technol., 140 (2015) 6–12.

[16] D.R. Manenti, P.A. Soares, A.N. Módenes, F.R. Espinoza-Quinones, Insights into solar photo-Fenton process using iron(III)–organic ligand complexes applied to real textile wastewater treatment, Chem. Eng. J., 266 (2015) 203–212.

[17] W.Y. Huang, M. Brigante, F. Wu, K. Hanna, G. Mailhot, Development of a new homogenous photo-Fenton process using Fe(III)-EDDS complexes, J. Photoch. Photobio. A., 239 (2012) 17–23.

[18] P. Piste, Cysteine-master antioxidant, Inter. J. Pharm. Chem. Biol. Sci., 3 (2013) 143–149.

[19] E.W. Iyamu, H. Perdew, G.M. Woods, Cysteine-iron promotes arginase activity by driving the Fenton reaction, Biochem. Biophys. Res. Commun., 76 (2008) 116–120.

[20] T. Li, Z.W. Zhao, Q. Wang, P.F. Xie, J.H. Ma, Strongly enhanced Fenton degradation of organic pollutants by cysteine: An aliphatic amino acid accelerator outweighs hydroquinone analogues, Water Res., 105 (2016) 479–486.

[21] L.S. Luo, Y.Y. Yao, F. Gong, Z.F. Huang, W.Y. Lu, Drastic enhancement on Fenton oxidation of organic contaminants by accelerating Fe(II)/Fe(III) cycle with L-cysteine, RSC. Adv., 6 (2016) 47661–47668.

[22] A.R. Yazdanbakhsh, A.S. Mohammadi, M. Sardar, H. Godini, M. Almasian, COD removal from synthetic wastewater containing azithromycin using combined coagulation and a Fenton-like process, Environ. Eng. Manag. J., 13 (2014) 2929–2936.

[23] A.R. Yazdanbakhsh, A.S. Mohammadi, A.A. Alinejad, G. Hassani, S. Golmohammadi, S.M. Mohseni, M. Sardar, V. Sarsangi, Reduction of non-Betalactamantibiotics COD by combined coagulation and advanced oxidation processes, Water. Environ. Res., 88 (2016) 2121–2131.

[24] X.J. Ma, H.L. Xia, Treatment of water-based printing ink wastewater by Fenton process combined with coagulation, J. Hazard. Mater., 162 (2009) 386–390.

[25] J. Zhang, S. Chen, Y. Zhang, X. Quan, H.M. Zhao, Reduction of acute toxicity and genotoxicity of dye effluent using Fenton-coagulation process, J. Hazard. Mater., 274 (2014) 198–204.

[26] L.H. Ai, C.H. Zhang, L.L. Li, J. Jiang, Iron terephthalate metal-organic framework: Revealing the effective activation of hydrogen peroxide for the degradation of organic dye under visible light irradiation, Appl. Catal. B-Environ., 148–149 (2014) 191–200.

[27] R. Li, C. He, Y.L. He, Preparation and characterization of poly-silicic-cation coagulants by synchronous-polymerization and co-polymerization, Chem. Eng. J., 223 (2013) 869–874.

[28] F. Ying, S.L. Yu, C.W. Han, Morphology and coagulation performance during preparation of poly-silicic-ferric (PSF) coagulant, Chem. Eng. J., 149 (2009) 1–10.

[29] T. Sun, C.H. Sun, G.L. Zhu, X.J. Miao, C.C. Wu, Preparation and coagulation performance of poly-ferric-aluminum-silicate-sulfate from fly ash, Desalination, 268 (2011) 270–275.

[30] N.D. Tzoupanos, A.I. Zouboulis, Novel inorganic-organic composite coagulants based on aluminum, Desal. Water Treat., 13 (2010) 340–347.

[31] A.M. Al-lbrahim, Seawater desalination: the strategic choice for Saudi Arabia, Desal. Water Treat., 51 (2013) 1–4.
[32.] Y. Fu, S.L. Yu, Y.Z. Yu, L.P. Qiu, B. Hui, Reaction mode between Si and Fe and evaluation of optimal species in poly-silicic-ferric coagulant, J. Environ. Sci., 19 (2007) 678–688.
[33.] Y.M. Fang, X.D. Zhao, X.L. Zhang, Study on the Image, structure and coagulation behavior of polysilicate-aluminum ferric, Ind. Saf. Environ. Prot., 33 (2007) 22–24.
[34.] S. Zinatlooajabshir, S. Mortazaviderazkola, M. Salavatiniasari, Simple sonochemical synthesis of HO_2O_3-SiO_2 nanocomposites as an effective photocatalyst for degradation and removal of organic contaminant, Ultrason. Sonochem., 39 (2017) 452–460.
[35.] K. Chen, Z. Bao, J. Shen, G. Wu, B. Zhou, Freestanding monolithic silicon aerogels, J. Mater. Chem., 22 (2012) 16196–16200.
[36.] R.F. Jameson, W. Linert, Complex formation followed by internal electron transfer: The reaction between cysteine and iron(III), Monatsh. Chem., 122 (1991) 887–906.
[37.] P.P. Gan, S.F.Y. Li, Efficient removal of Rhodamine B using a rice hull-based silica supported iron catalyst by Fenton-like process, Chem. Eng. J., 229 (2013) 351–363.
[38] X.L. Liang, Y.H. Zhong, H.P. He, P. Yuan, J.X. Zhu, The application of chromium substituted magnetite as heterogeneous Fenton catalyst for the degradation of aqueous cationic and anionic dyes, Chem. Eng. J., 191 (2012) 177–184.
[39] M.A. Behnajady, N. Modirshahla, F. Ghanbary, A kinetic model for the decolorization of C.I. Acid Yellow 23 by Fenton process, J. Hazard. Mater., 148 (2007) 98–102.
[40] M. Tamimi, S. Qourzal, N. Barka, A. Assabbane, Y. Ait-Ichou, Methomyl degradation in aqueous solutions by Fenton's reagent and the photo-Fenton system, Sep. Purif. Technol., 61 (2008) 103–108.
[41] A. Amirbahman, L. Sigg, U. Gunten, Reductive dissolution of Fe(III) (Hydr)oxides by Cysteine: kinetics and mechanism, J. Colloid. Interf. Sci., 194 (1997) 194–206.